Journal of Systems Engineering and Electronics
Vol. 35, No. 4, August 2024, pp.987 – 998

Method of improving pedestrian navigation performance based on chest card

CHENG Hao[1], GAO Shuang[1], CAI Xiaowen[2], WANG Yuxuan[1,*], and WANG Jie[3]

1. School of Instrumentation and Optoelectronic Engineering, Beihang University, Beijing 100191, China;
2. School of Automation and Electronic Information , Xiangtan University, Xiangtan 411105, China;
3. Navigation Guidance and Control, Graduate School of the Second Institute of China Aerospace Science and Industry Corporation, Beijing 100854, China

Abstract: With the development of positioning technology, location services are constantly in demand by people. As a primary location service pedestrian navigation has two main approaches based on radio and inertial navigation. The pedestrian navigation based on radio is subject to environmental occlusion leading to the degradation of positioning accuracy. The pedestrian navigation based on micro-electro-mechanical system inertial measurement unit (MIMU) is less susceptible to environmental interference, but its errors dissipate over time. In this paper, a chest card pedestrian navigation improvement method based on complementary correction is proposed in order to suppress the error divergence of inertial navigation methods. To suppress attitude errors, optimal feedback coefficients are established by pedestrian motion characteristics. To extend navigation time and improve positioning accuracy, the step length in subsequent movements is compensated by the first step length. The experimental results show that the positioning accuracy of the proposed method is improved by more than 47% and 44% compared with the pure inertia-based method combined with step compensation and the traditional complementary filtering combined method with step compensation. The proposed method can effectively suppress the error dispersion and improve the positioning accuracy.

Keywords: pedestrian navigation, micro-electro-mechanical system (MEMS), inertial navigation, complementary filtering.

DOI: 10.23919/JSEE.2024.000084

1. Introduction

With the development of satellite communication and navigation technology, pedestrian location service has become an essential safety and security technology, which is widely used in many fields such as security of large exhibitions, firefighting, border patrol and field mapping [1]. Take firefighting operation as an example, its operation site is affected by firelight and smoke, which makes it difficult to confirm the operator's own position and affects firefighting efficiency or even safety accidents. There is an urgent need to develop low-cost pedestrian navigation and positioning technology that is not constrained by the use of the environment, which can support operators to complete special tasks efficiently and safely.

The current pedestrian navigation and positioning methods are divided into two main categories. The first category is passive pedestrian navigation, including ultra-wideband (UWB) [2,3], bluetooth low energy (BLE) [4,5], satellite navigation [6], and other radio positioning methods. Passive pedestrian navigation is susceptible to interference from complex environments. For example, local radio base station signals are susceptible to multipath effects and non-visual range errors, leading to large errors in navigation and positioning [7–9]. Satellite navigation cannot be located due to occlusion [10]. The second category is active pedestrian navigation, including geomagnetic navigation [11], and inertial navigation [12]. The geomagnetic navigation in active pedestrian navigation methods can only be used for orientation and cannot provide complete navigation information. Inertial navigation can provide highly accurate position recurrence results in a short period of time and is not easily affected by environment. However, the errors will accumulate over time. With the development of micro-electro-mechanical system (MEMS), MEMS process-based inertial devices have significant advantages in small size, low cost and easy integration. Therefore, adding effective error suppression methods, the pedestrian navigation method based on MEMS inertial devices will have great advantages.

Manuscript received March 13, 2023.
*Corresponding author.

In order to ensure that the micro-electro-mechanical system inertial measurement unit (MIMU) based pedestrian navigation method can maintain effective positioning accuracy for a long time, scholars have started their research in the direction of navigation error suppression and wearing methods.

The navigation errors are mainly suppressed from zero velocity correction [13–15], magnetic heading constraint, gait recognition, and pedometer. For the zero velocity correction method, it is difficult to set the zero velocity threshold. Wang et al. [16] designed an adaptive threshold zero-speed detector. The adaptive threshold in the likelihood ratio test is determined by Bayesian principle. And the detector can be applied to different motor gaits without specific settings of parameters. For the magnetic heading constraint methods, magnetic interference directly affects the detection of magnetic field information. Hu et al. [17] analyzed a model of the effect of magnetic disturbance fields on the spatial distribution of the geomagnetic field. Two non-normal magnetic field features to distinguish between normal magnetic fields and the presence of interference were found. Therefore, in order to extract normal magnetic data from distorted data, a decision tree is trained by two feature-based classification regression tree algorithms. For the step correction method, it is important to measure the step information effectively. Deng et al. [18] proposed a body odometer (BOR) algorithm to improve the step model. To correct for step size, body-related correction factors are added to the traditional compensation estimation model, resulting in more accurate calculation of step size. The core of the navigation error suppression is the addition of new filtered observations. As in the sub-curve constraint, the heading angle error is suppressed by the magnetic field information during the motion. As in pedometer calibration, velocity and position errors are suppressed by the time and distance of a single step movement. There is an impact on size and cost by increasing the number of sensors required to add an external source of valid information. Inertial navigation based on complementary filtering [19,20] has complementary advantages due to the inconsistency of acceleration and angular velocity on dynamic response characteristics. Therefore, this paper will be based on complementary filtering method of inertial pedestrian navigation research.

Wearing methods mainly include foot wear, double foot wear, and multi-sensor wear. To improve the navigation accuracy, high precision step measurement methods through different wearing methods are investigated. Li et al. [21] used dual sensors placed on the foot to construct foot vectors whose relative position relationship does not change with the lower extremity segment. And this relative position relationship is used to construct a Kalman filter that fuses position-velocity observations. Laverne et al. [22] improved the heading accuracy by installing an intertial measurement unit (IMU) on each foot of the pedestrian, and there exists a maximum movement distance due to the limitation of legs and torso during the movement of both feet. The system is limited by this maximum movement distance. Most of the solutions for non-foot-worn solutions are based on multi-sensor combinations for navigation and error suppression by multiple measurement information. Tjhai et al. [23] used multisensor multiplexing by placing a total of seven IMUs on the foot, calf, thigh and torso, so as to simulate the pedestrian's lower limb kinematic features during the movement. However, due to the foot-worn scheme, where the sensors are mounted directly on the foot, the impact during pedestrian motion will be directly reflected to the sensors, which leads to errors that can disperse rapidly. The non-foot-worn solutions also all require multiple sensors to measure together, increasing the cost and difficulty of use.

In this paper, starting from the error dispersion mechanism of inertial devices and combining with the law of pedestrian kinematics, a pedestrian inertial navigation and positioning scheme based on the chest card wearing method is proposed. There are three innovations.

(i) The footed wearing method leads to sensitive high dynamic angular motion of inertial devices, which makes the inertial device performance deteriorate rapidly. The proposed chest card wearing method can circumvent the high dynamic angular motion and directly improve the inertial device navigation performance.

(ii) Compared with the traditional zero-speed detection correction method which can only correct errors at static time points, the introduced complementary filtering performs navigation error correction throughout the travel and extends the inertial navigation time.

(iii) The transfer function is established based on the pedestrian navigation error mechanism, and the optimal selection of the complementary filtering closed-loop feedback parameters is performed based on the characteristics of the navigation method.

2. Pedestrian kinematic characteristics analysis

Traditional foot-worn pedestrian inertial navigation errors dissipate rapidly over time, mainly due to the accumulation of posture errors under the excitation of high dynamic angular motion and the high impact of foot con-

tact with the ground resulting in drastic changes in acceleration information. Chest card pedestrian navigation effectively uses the stability of the human center of gravity during walking to circumvent the effects of high dynamic angular motion and sharp changes in acceleration under impact, which is beneficial to high-precision navigation. However, due to the short zero velocity interval, it is difficult for zero velocity correction. Therefore, in this section pedestrian acceleration and deceleration kinematic characteristics are analyzed by data from real walking processes. The navigation error correction method will be mined based on pedestrian motion characteristics.

2.1 Kinematic characteristics of pedestrian acceleration and deceleration

The acceleration and velocity profiles of real pedestrian motion under the navigation system are shown in Fig. 1. It can be seen that when the pedestrian is in motion, the fluctuation of the up and down of the badge-type tag is small. Thus the acceleration in the sky direction basically remains balanced. The motion characteristics are mainly reflected in the horizontal motion. The horizontal motion generally shows the motion characteristics of forward or rotation without lateral movement. Acceleration and velocity curves can be seen in the normal a walking process presents three parts of accelerated motion, approximately uniform motion, and decelerated motion. Since the pedestrian motion is stable in the intermediate phase, the motion acceleration is small relative to the gravitational acceleration under the calculation of integration with a period greater than the step length. Therefore, the acceleration of the intermediate stage is approximated by the acceleration of gravity, which means that the whole process is approximately uniform motion. That is, during the whole pedestrian motion, the motion can be decomposed into single-step motion components, and the acceleration under each single-step motion cycle shows a periodic variation, indicating that the mean value of the acceleration projected under navigation should theoretically be approximately equal to the gravitational acceleration. Thus based on this feature, it is possible to correct the error of the whole navigation by the stability characteristic of its acceleration throughout the motion.

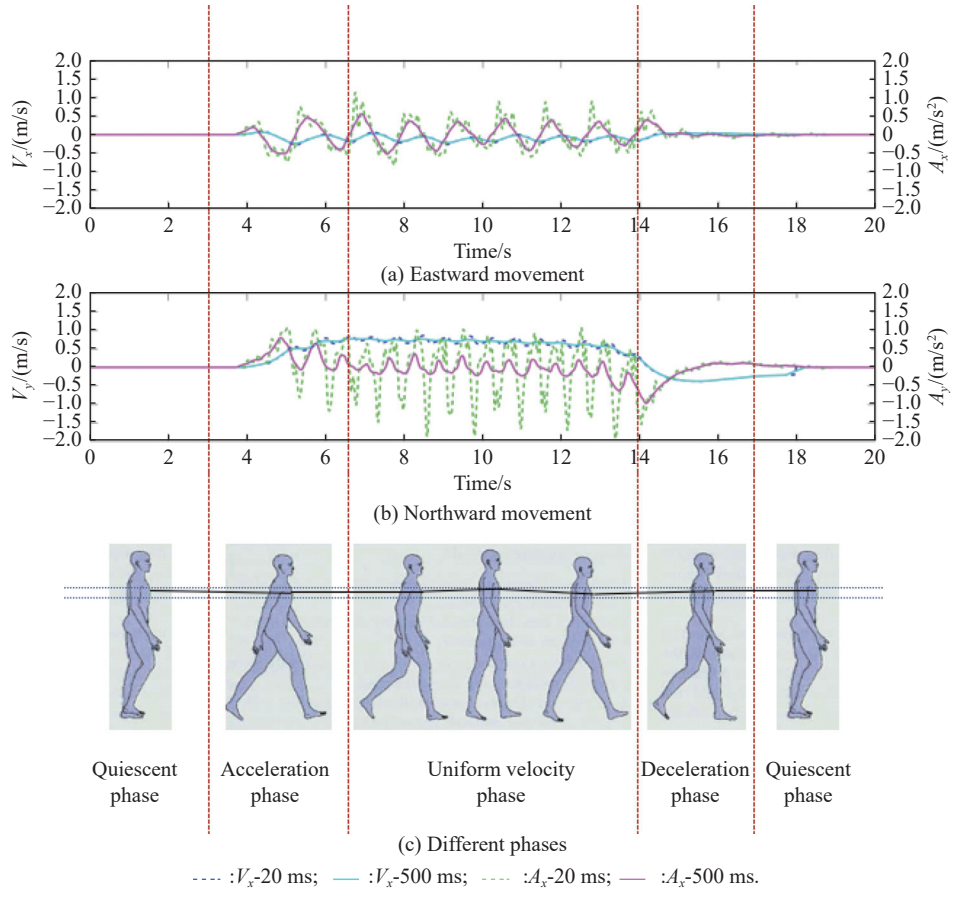

Fig. 1 Pedestrian movement characteristics map

2.2 Analysis of attitude compensation based on complementary filtering

Through the above analysis of pedestrian motion characteristics, it can be seen that the pedestrian motion process is mainly out of the approximate uniform motion state. The accelerometer basically maintains a constant value under the long-period integration condition. Therefore, inspired by the complementary filtering method, a complementary filtering method for chest card pedestrian navigation is proposed in this paper. The gyroscopic integration error can be effectively constrained by this method which is effective in suppressing the position error caused by attitude error. The basic principle is that the acceleration measured by IMU during walking is dominated by gravitational acceleration, and the disturbing acceleration of pedestrian motion can be smoothed to much less than gravitational acceleration during long-period integration. In turn, the attitude error can be corrected by the acceleration. Attitude errors are reflected by measuring the projection of the acceleration vector under the navigation system and the degree of non-coherence of the gravitational acceleration vector. Then it is fed back to the navigation solution by means of damping to achieve the attitude error divergence suppression effect. That is, the angular error of the two vectors of motion acceleration and gravitational acceleration is $\boldsymbol{\delta}$. Then, it can be compensated by the feedback $K\cdot\boldsymbol{\delta}$ coefficient into the calculation of angular velocity in the solution, so as to correct the attitude, where $K\leqslant 1$.

The traditional complementary filtering method can only have a good error suppression effect under stationary or uniform motion. In pedestrian navigation, the main motion is non-homogeneous motion, therefore, this method averages the acceleration in a single step motion cycle, and the mean value should be approximately equal to the gravitational acceleration, so that the posture error can be observed and compensated by this motion characteristic to achieve the effect of complementary filtering.

3. Chest card pedestrian navigation method based on complementary correction algorithm

3.1 Pedestrian navigation method scheme

The scheme of the pedestrian navigation method designed in this paper consists of five modules: state detection, static correction, dynamic navigation, dynamic complementary filtering, and dynamic step length compensation. State detection is used to determine the current state. Static correction is used to eliminate the accumulated errors of navigation. Dynamic navigation serves to solve the current motion information in real time. Complementary filtering corrects for attitude errors based on accelerometer information. Step length compensation suppresses the long time position solving dispersion problem by step information.

3.1.1 Status detection

The mean values of the measured values of the MEMS gyroscope and MEMS accelerometer at the selected time T, remove certain random noise interference.

$$\begin{cases}\dfrac{1}{k}\displaystyle\sum_{i=1}^{k}|\boldsymbol{f}_i|-|\boldsymbol{g}|<\varepsilon_{\text{acc}}\\ \dfrac{1}{k}\displaystyle\sum_{i=1}^{k}|\boldsymbol{\omega}_i|<\varepsilon_{\text{gyro}}\end{cases}\tag{1}$$

where $\boldsymbol{f}_i$ is the current accelerometer measurement, $\boldsymbol{g}$ is the gravitational acceleration, $\boldsymbol{\omega}_i$ is the gyro measurement, ε_{acc} is the acceleration condition to determine if it is static, and $\varepsilon_{\text{gyro}}$ is the angular velocity velocity condition to determine if it is static.

3.1.2 Static correction

In this method, the zero offset of the gyroscope and the scale of the accelerometer are calculated in the static part to compensate the inertial device with an online calibration, thus extending the navigation time of the inertial device.

$$\begin{cases}\mathbf{gB}=\dfrac{1}{k}\displaystyle\sum_{i=1}^{k}\boldsymbol{\omega}_i\\ \text{aSF}=\left|\dfrac{1}{k}\displaystyle\sum_{i=1}^{k}\boldsymbol{f}_i\right|\end{cases}\tag{2}$$

where **gB** is to calculate the zero offset of the three-axis gyro and aSF is to calculate the accelerometer scale.

The attitude angle of the system is determined by the acceleration information, which is calculated as

$$\begin{bmatrix}f_x\\ f_y\\ f_z\end{bmatrix}=\boldsymbol{C}_b^n\cdot\begin{bmatrix}0\\ 0\\ g\end{bmatrix}=\begin{bmatrix}g\cdot\sin\gamma\cdot\cos\vartheta\\ -g\cdot\sin\vartheta\\ -g\cdot\cos\gamma\cdot\cos\vartheta\end{bmatrix}\tag{3}$$

where ϑ is the pitch angle, γ is the cross-roll angle, and $\boldsymbol{C}_b^n$ is the attitude matrix.

Assuming an initial heading of zero degrees, the current quaternion $\boldsymbol{Q}$ and the strapdown attitude matrix $\boldsymbol{C}_b^n$ can be calculated based on the desired horizontal attitude angle and used for subsequent navigation solving.

The attitude matrix can be obtained from the calculated initial quaternions as

$$\begin{cases}\boldsymbol{P}_i^n=\boldsymbol{P}_{i-1}^n\\ \boldsymbol{V}_i^n=\mathbf{0}\end{cases}\tag{4}$$

where $\boldsymbol{P}^n$ is the position and $\boldsymbol{V}^n$ is the velocity.

3.1.3 Dynamic navigation

Calculate the angular velocity in the current state of motion. The angular velocity measured by the gyroscope includes the inherent gyro zero bias. The method proposed in this paper is to correct the attitude error by compensating the feedback to the angular velocity of motion in the form of equivalent gyro zero bias, and the angular velocity of motion is as

$$\boldsymbol{\omega}_{nb}^{b} = \boldsymbol{\omega} - \mathbf{gB} - \boldsymbol{\alpha} \tag{5}$$

where **gB** is the zero bias of the three-axis gyro obtained in the static state, $\boldsymbol{\omega}$ is the measured angular velocity, and $\boldsymbol{\alpha}$ is the equivalent zero bias value corresponding to the feedback in this paper. b and n denote the carrier system and the navigation system, respectively.

After obtaining the determined angular velocity of the motion, the quaternion is updated by integrating the actual angular velocity change.

$$\boldsymbol{Q}_i = \boldsymbol{Q}_{i-1} + \frac{1}{2}\boldsymbol{\Omega}_{nb}^{b} \cdot \boldsymbol{Q}_{i-1} \cdot \mathrm{dt} \tag{6}$$

where $\boldsymbol{\Omega}_{nb}^{b}$ is the antisymmetric matrix formed by the angular velocity of the three axes and dt is the navigation time.

After obtaining the quaternion in the current state, the attitude matrix $\boldsymbol{C}_b^n$ can be updated according to the quaternion.

The acceleration measured by the accelerometer is projected to a fixed navigation coordinate system through the attitude matrix, and the effect of gravitational acceleration is removed in the navigation coordinate system to obtain the real acceleration of the object motion.

$$\boldsymbol{f}^n = \boldsymbol{C}_b^n \cdot \boldsymbol{f}^b + \boldsymbol{g}^n \tag{7}$$

where $\boldsymbol{f}^n$ is the acceleration under the navigation system.

The velocity and position changes under the navigation system are calculated based on the obtained acceleration information under the navigation system. Its velocity variation is

$$\boldsymbol{V}_i^n = \boldsymbol{V}_{i-1}^n + \frac{1}{2}(\boldsymbol{f}_i^n + \boldsymbol{f}_{i-1}^n) \cdot \mathrm{dt} \tag{8}$$

where $\boldsymbol{V}_i^n$ is the speed under the current navigation system.

The position changes to

$$\boldsymbol{P}_i^n = \boldsymbol{P}_{i-1}^n + \boldsymbol{V}_i^n \cdot \mathrm{dt}. \tag{9}$$

3.1.4 Improved error compensation for complementary filtering methods

The mean value of the projection of the accelerometer measurement under the navigation system at time t is compared with the gravitational acceleration under the navigation system. The attitude error is reflected by the degree of non-coincidence of these two vectors. Therefore, the angular error formed by this non-overlap is multiplied by a feedback coefficient which is used as an equivalent zero-bias compensation for angular velocity to eliminate the attitude error, thus realizing the error compensation for pedestrian navigation and improving the navigation accuracy. The specific implementation method is as follows.

First, the accelerometer measurements are projected on the navigation system, and the mean value of time is calculated to construct the motion acceleration vector.

$$\bar{\boldsymbol{f}}^n = \frac{1}{k}\sum_{i=1}^{k} \boldsymbol{f}^n \tag{10}$$

where $\bar{\boldsymbol{f}}^n$ is the mean value of the projection of the ratio at time t under the navigation system.

Then the non-linearity of the two vectors is obtained by fork multiplication of gravitational acceleration and motion acceleration.

$$\boldsymbol{e}^n = \boldsymbol{g}^n \otimes \bar{\boldsymbol{f}}^n \tag{11}$$

where $\boldsymbol{e}^n$ is the result of two vector fork multiplication, and $\otimes$ is the vector cross product.

The fork multiplication result reflects the attitude error, so it is necessary to compensate this result into the attitude solution. The method in this paper is to compensate into the angular velocity in the form of zero bias, so as to suppress the attitude error, and its compensation zero position is

$$\boldsymbol{\alpha} = \frac{\partial(\boldsymbol{C}_n^b \cdot \boldsymbol{K} \cdot \boldsymbol{e}^n)}{\partial(\mathrm{dt})} \tag{12}$$

where $\boldsymbol{K}$ is the optimal feedback compensation coefficient matrix.

3.1.5 Step length compensation

In order to suppress the error dispersion problem of long-time navigation of inertial devices, this paper adopts the method of step length compensation, which compensates the single step length in subsequent walks according to the step length solved in the first step, and its compensation formula is

$$L_i = L_i' + s \cdot (L_0 - L_i') \tag{13}$$

where L_0 and L_i are the first step and current step, respectively, L_i' is the solved displacement, and s is a compensation factor related to pedestrian body parameters.

In summary, the algorithm scheme proposed in this paper is specified in Fig. 2.

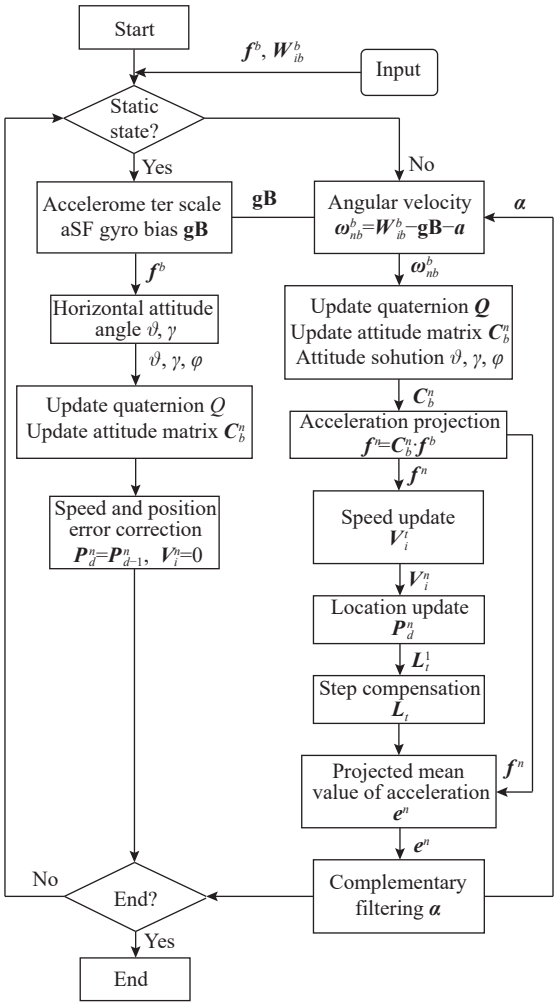

Fig. 2 Scheme chart of chest card complementary correction pedestrian navigation method

3.2 Optimal K value selection

The complementary filtering process is described in the previous Subsection 3.1.4, and the following section will analyze the complementary filtering method from the principle and the selection of the optimal feedback coefficient matrix $\boldsymbol{K}$ value. To simplify the analysis, in this section, the feedback coefficient matrix $\boldsymbol{K}$ is reduced to the feedback coefficients K for error feedback compensation under a single link.

The block diagram of the system of the complementary filtering method is shown in Fig. 3. The improved complementary filtering method proposed in this paper calculates the current existed attitude error by time t plus table mean and gravitational acceleration, and compensate the attitude error by differentiating it in time as a combination of zero bias and zero bias of the gyro itself into the navigation solution.

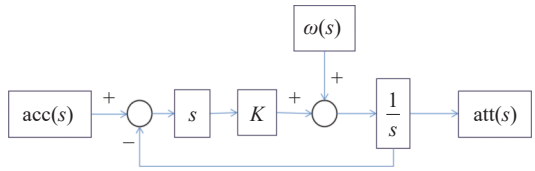

Fig. 3 Block diagram of error transfer of complementary filtering system

Therefore the error transfer process is shown in Fig. 3 and the error transfer function can be written as

$$\mathrm{att}(s)=\frac{K\cdot\mathrm{acc}(s)\cdot s+\omega(s)}{s\cdot(1+K)} \tag{14}$$

where att(s) is the attitude error, acc(s) is the acceleration error, and $\omega(s)$ is the angular velocity error.

Since the gyro zero bias error and accelerometer motion error in the process of movement are not related to time, the attitude error calculated by the maximum plus table can be taken as $\delta\theta_{\mathrm{acc}}$; at the same time, the gyro zero bias is a certain value during the single power-up operation, which is not related to time, and the gyro zero bias error can be $\delta\theta_g$. Therefore, the transfer function can be rewritten as

$$\mathrm{att}(s)=\frac{K\cdot\delta\theta_{\mathrm{acc}}\cdot s+\delta\theta_g}{s+K\cdot s}. \tag{15}$$

The amplitude and frequency characteristics of the transfer function are as

$$A(\omega)=\frac{\sqrt{\delta\theta_g{}^2+(K\cdot\delta\theta_{\mathrm{acc}})^2\cdot\omega^2}}{(1+K)\cdot\omega}. \tag{16}$$

Therefore, the objective function is set according to the amplitude and frequency characteristics:

$$\delta\theta=\frac{\sqrt{\delta\theta_g{}^2+(K\cdot\delta\theta_{\mathrm{acc}})^2\cdot\omega^2}}{(1+K)\cdot\omega} \tag{17}$$

where $\delta\theta$ is the attitude error, $\delta\theta_g$ is the gyro zero bias error, and $\delta\theta_{\mathrm{acc}}$ is the acceleration error.

Because in the amplitude frequency characteristics $\omega=2\pi f=2\pi/T$, therefore the objective function can be rewritten as

$$\delta\theta=\frac{\sqrt{(\delta\theta_g\cdot T)^2+(2\pi\cdot K\cdot\delta\theta_{\mathrm{acc}})^2}}{2\pi\cdot(1+K)}. \tag{18}$$

3.2.1 Upper bound on the value of K

The core of the improved complementary filtering method used in this paper is to use acceleration information to correct attitude error. The minimum attitude error compensated by this method is the attitude error calculated from the accelerometer device accuracy. And the maximum attitude error is the attitude error calculated from the motion acceleration in the accelerometer only.

That is, the compensation of attitude error is related to

the integration error of motion acceleration and gyro zero bias first, where the larger the value of K, the greater the attitude error caused by the motion acceleration, the gyroscope zero bias integration error will be reduced instead. Therefore, if K=1, it can be considered that the attitude error is all caused by the motion acceleration; and when K>1, the attitude error will become larger with the increase of K value, and cannot achieve the attitude error suppression effect we want. Therefore, $K \leqslant 1$,

$$K_{\max} = 1. \tag{19}$$

3.2.2 Lower bound constraint on the value of K

The lower limit of the feedback coefficient K value is determined by the angular velocity integration error measured by the gyro together with the disturbance acceleration, at this feedback coefficient K, the integrated error is less than the attitude error calculated using only the acceleration.

Suppose, the disturbance acceleration error is $\delta\theta_{\text{acc}}$ and the gyro integration error is $\int \delta\theta_g \cdot \mathrm{d}t$, then the lower limit of K value is

$$K_{\min} = G(\delta\theta_{\text{acc}}, \delta\theta_g, t). \tag{20}$$

The function G represents the relationship between the feedback coefficient K and the convergence time t.

3.2.3 Simplified analysis of convergence time

The convergence time is defined here as the time used to compensate for the error when the feedback compensation coefficient K exists, and the party error converges to an acceptable range. Therefore, the relationship between convergence time and feedback coefficient K can be obtained through the following simplified simulation, where convergence time is directly related to the magnitude of gyro zero bias integration error, and feedback coefficient is directly related to the magnitude of attitude error caused by motion acceleration. This will lay the analytical foundation for the subsequent analysis of the optimal feedback coefficient K corresponding to the minimum attitude error.

The concept of convergence time of this method is introduced here. Suppose the initial error is δ and the value is the correction factor K. Then the time required when the error converges to $1/x$ of the original error is the convergence time.

$$\mathrm{err}_i = \mathrm{err}_{i-1} - \mathrm{err}_{i-1} \cdot K, \tag{21}$$

when

$$\sum_{i=1}^{n} 1 \cdot K + \mathrm{err}_i \cdot K > \frac{x-1}{x}\delta \text{ or } \mathrm{err}_i < \frac{1}{x}\delta \tag{22}$$

where err_i is the corrected error.

3.2.4 Numerical method of optimal value solving

According to the above simplified convergence time model, assuming that the initial error is 1, the convergence condition is that the error converges to the original error, for the correction coefficient [0.001:0.001:1], and the correction frequency is 50 Hz, the simulation is carried out to obtain the relationship between the correction coefficient K and the convergence time, and the results are shown in Fig. 4.

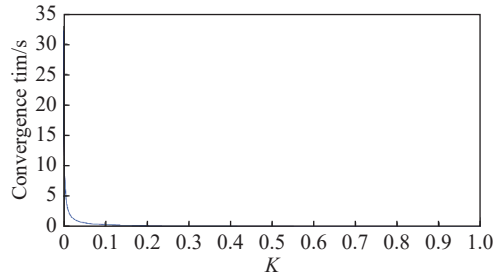

Fig. 4 Relationship between K value and convergence time

Then giving the arithmetic example obtained from real data, the acceleration of motion of the accelerometer is 2.916 m/s^2, the attitude error calculated from the acceleration of motion is $\delta\theta_{\text{acc}} = 16.530\,6°$, the zero offset error of the gyro is $\delta\theta_g = 0.141\,2\,°/\text{s}$, K=[0.000 01:0.000 1:1], the simulation is performed according to the objective function, and the results of attitude error and feedback coefficient are obtained as shown in Fig. 5.

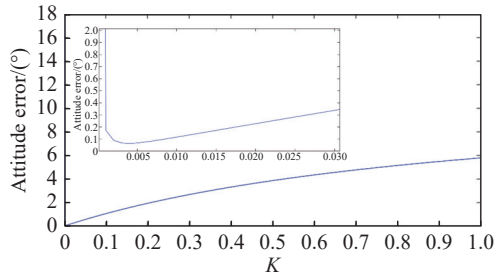

Fig. 5 Simulation results of K value and attitude error

The relationship between the value and the attitude error is shown in Fig. 6.

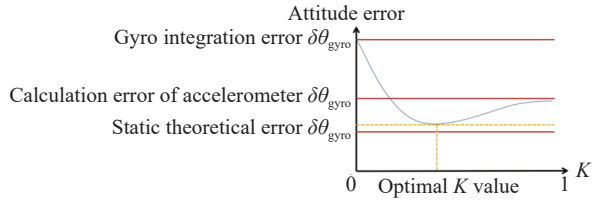

Fig. 6 Relationship between K value and attitude error

4. Experiment and result

The IMU used in the experiment is ICM20602. Its specific performance parameters are shown in Table 1. The test scenario is an outdoor open field, walking along a rectangular garden, keeping the walking speed at 1.0−1.5 m/s and stopping briefly at the turn for alignment correction. The following will compare the pure inertia with step length compensation solution method (PIWSLCS), the traditional complementary filtering with step length compensation method (TCFWSLC), and the improved method in this paper based on improved complementary filtering with step length compensation (ICFWSLC).

Table 1 Experimental equipment parameters

Device	Performance	Value
Gyroscope	Zero bias stability/(°/s)	0.04
	Scale factor nonlinearity/ppm	⩽ 1 000
	Noise factor/(μg/ $\sqrt{\text{Hz}}$)	100
Accelerometer	Zero bias stability/mg	1
	Scale factor nonlinearity/ppm	⩽ 3 000
	Noise factor/(μg/ $\sqrt{\text{Hz}}$)	100

The results of five trials are recorded in Table 2. All five of which involve a wrap-around walk along a rectangular area and a static realignment with a standing stop at each turn. In the rectangular area, preset points are set at 0.5 m intervals for real trajectory recording, each single-step motion walk is performed according to the preset points. And stand still at each turn to keep the device approximately immobile, thus re-aligning and eliminating some error accumulation.

Table 2 Experimental results statistics m

Case	Distance traveled	PIWSLCS	TCFWSLC	ICFWSLC
1	32	2.48	1.86	1.07
2	44	4.95	5.72	2.01
3	46	3.94	3.75	2.08
4	48	4.08	3.61	1.29
5	45	6.55	3.98	2.05

Table 2 records the total motion mileage of the five trials and the positioning error of the final point, which is used to judge the positioning effectiveness of the three methods. The positioning error equation is

$$\Delta p = \sqrt{(x_{\text{last}} - x_{\text{true}})^2 + (y_{\text{last}} - y_{\text{true}})^2} \tag{23}$$

where Δp is the final point positioning error, $(x_{\text{last}}, y_{\text{last}})$ is the final point positioning coordinate, and $(x_{\text{true}}, y_{\text{true}})$ is the true coordinate.

Walking trajectories calculated by the three methods are shown in Fig. 7. As can be seen from the figure due to walking, the IMU has been in motion, and cannot be installed in the foot sensor can be zero velocity correction when the foot stays on the ground, which leads to the rapid accumulation of error in the solution of PIWSLCS, the final position error is a maximum of 6.55 m. Although the error can be suppressed by using TCFWSLC, the presence of error is still large, the maximum of 5.72 m. ICFWSLC based on the pedestrian motion model, enhances accuracy by constraining step size with step length and the maximum position error is 2.08 m, which is significantly smaller than the other two methods.

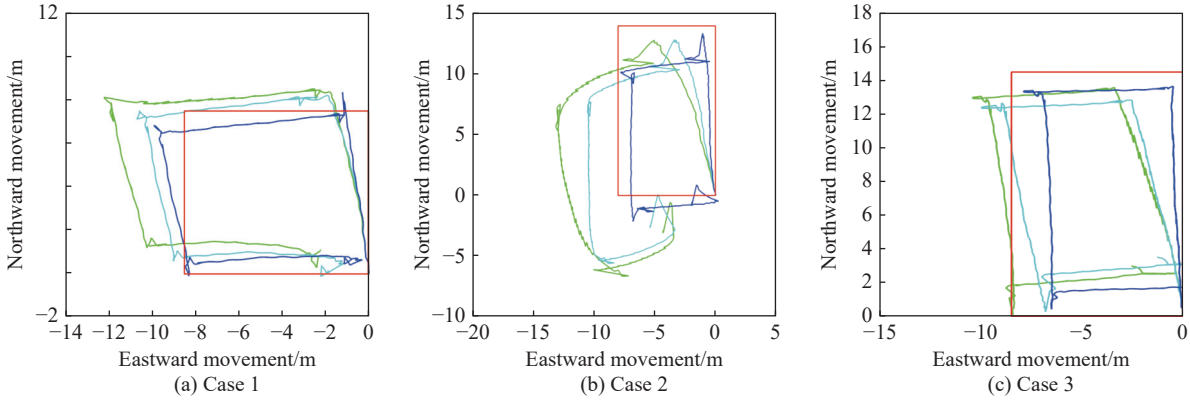

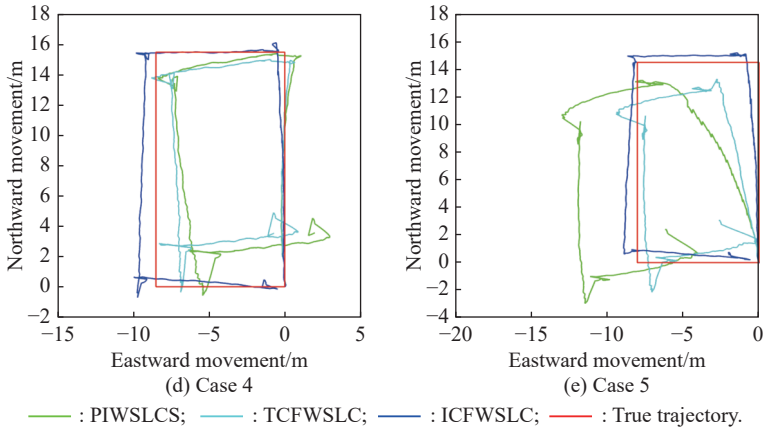

Fig. 7 Results of five cases

The specific analysis for case 1. The positioning error of the three methods comparing the real trajectory when each footstep is selected to land are shown in Fig. 8. That is, the positioning error is calculated by comparing the single-step positioning points solved by each method with the preset real trajectory points, and the positioning error formula is

$$\Delta p = \sqrt{\frac{1}{n}\sum_{i=1}^{n}\left[(x_i - x_{i-\text{true}})^2 + (y_i - y_{i-\text{true}})^2\right]} \tag{24}$$

where Δp is the final point positioning error, (x_i, y_i) is the positioning coordinates of each single-step motion point, and $(x_{i-\text{true}}, y_{i-\text{true}})$ is the true coordinates of each single-step motion point.

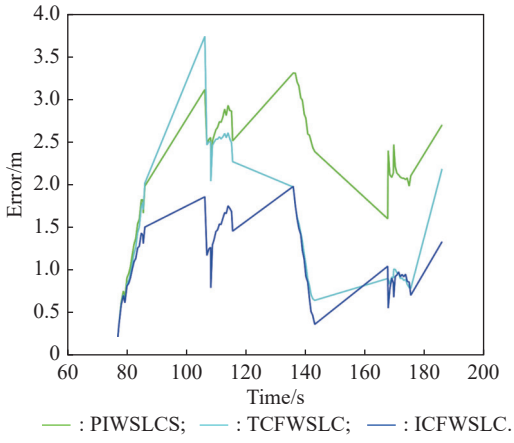

Fig. 8 Positioning error

It can be seen that the positioning error of the proposed method is significantly smaller than the other two methods, and the final positioning error of the proposed method is 1.19 m, while that of the other two methods is 2.31 m and 1.69 m, with an improvement of 48% and 30% in positioning accuracy. The experimental results show that the proposed method has a large improvement in the positioning performance.

Estimation plots with different feedback coefficients $\boldsymbol{K}$ are shown in Fig. 9. The optimal $\boldsymbol{K}$ (represents a vector of compensation coefficients consisting of feedback compensation coefficients for the three attitude angles) value is calculated as [0.000 013 0.000 043 0.000 01] according to the above Subsection 3.2.4, the parameter of non-optimal $\boldsymbol{K}$ value 1 is [0.000 053 0.000 083 0.000 01], and the parameter of non-optimal $\boldsymbol{K}$ value 2 is [0.000 003 0.000 003 0.000 01]. It can be seen that the selection of feedback coefficient directly determines the size of the compensation, and the non-optimal feedback coefficient will make the compensation too large or too small and lead to large positioning deviation.

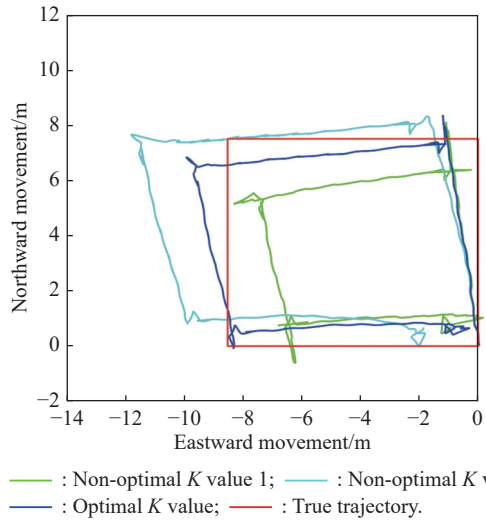

Fig. 9 Trajectory plots for different K values

Fig. 10 shows the velocity curves in the east direction and north direction during the motion. The blue curve is the method proposed in this paper, and it can be seen that

the velocity should theoretically be 0 m/s at that moment of stopping before the turn, and the comparison can show that the velocity error of the proposed method is the smallest, which can show that the proposed method can effectively suppress the divergence of velocity error.

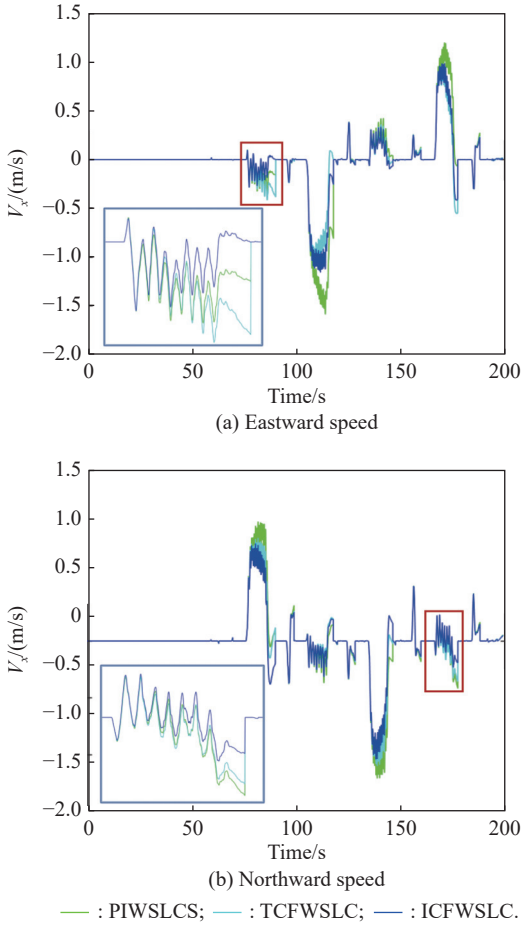

Fig. 10 Horizontal speed comparison

Fig. 11 shows the change of attitude angle during the motion, as this experiment uses a single MIMU device without attitude standard. However, the attitude error will be reflected in the velocity and position error, so from the position-velocity results in Fig. 7 and Fig. 10, it can be seen that the method proposed in this paper can correct the attitude error, so as to maintain the attitude stability and thus maintain the positioning accuracy for a long time.

The experimental results show that the positioning accuracy of the proposed method is improved by more than 47% and 44% compared with PIWSC and TCFWSC, respectively, which can effectively suppress the error dispersion caused by the inability of zero velocity correction for single-step walking and improve the positioning accuracy.

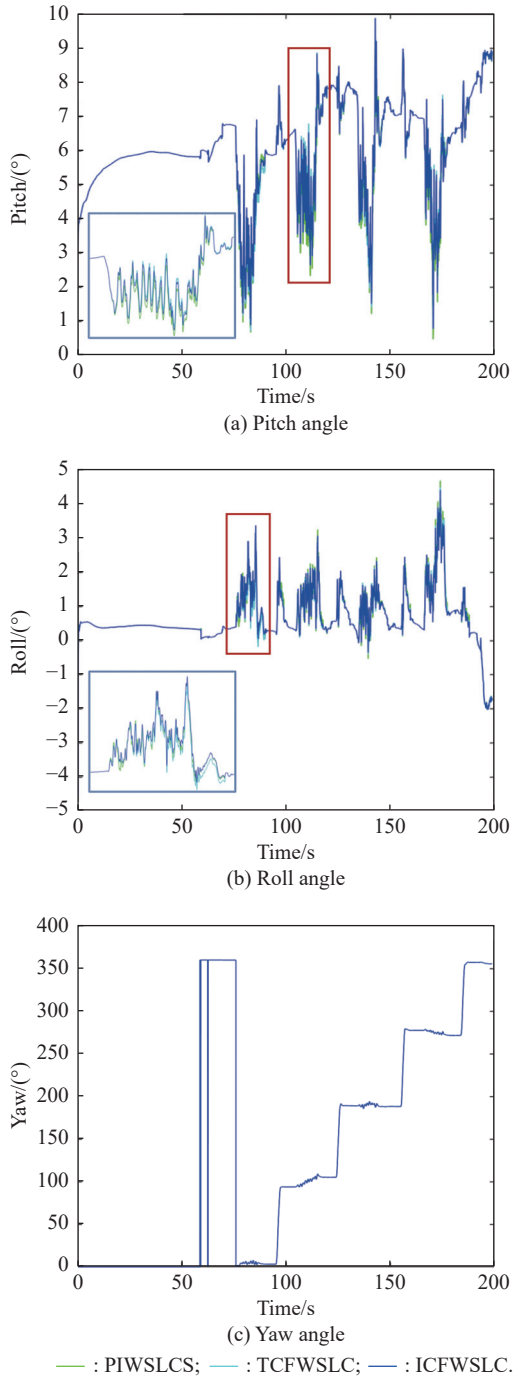

Fig. 11 Attitude comparison

5. Conclusions

In this paper, a chest card pedestrian navigation method based on full fusion complementary filtering is proposed. The chest card wearing method circumvents the problem of rapid dispersion of pose due to high dynamic angular motion caused by the impact in the footplate wearing method. Moreover, the traditional complementary filtering method is improved for the pedestrian characteristics

of the chest card position. And the optimal feedback gain is designed based on the error mechanism generated by the pedestrian motion, so that the error is suppressed and the navigation time is improved. The experimental results show that the proposed method can effectively suppress the attitude and velocity dispersion and thus improve the positioning accuracy compared with the traditional pure inertial method and the complementary filtering method. Its positioning accuracy has been improved by 47% and 44%, which can effectively suppress attitude and velocity dispersion to improve positioning accuracy and navigation time to a certain extent. This method has a strong application value for consumer-level inertial pedestrian navigation solutions.

References

[1] ALSHAMI I H, AHMAD N A, SAHIBUDDIN S, et al. Adaptive indoor positioning model based on WLAN-fingerprinting for dynamic and multi-floor environments. Sensors, 2017, 17(8): 1789.

[2] KOLAKOWSKI J, DJAJA-JOSKO V, KOLAKOWSKI M, et al. UWB/BLE tracking system for elderly people monitoring. Sensors, 2020, 20(6): 1574.

[3] LIU F, ZHANG J X, WANG J, et al. An UWB/vision fusion scheme for determining pedestrians' indoor location. Sensors, 2020, 20(4): 1139.

[4] FARAGHER R, HARLE R. Location fingerprinting with bluetooth low energy beacons. IEEE Journal on Selected Areas in Communications, 2015, 33(11): 2418–2428.

[5] ABDULRAHMAN A, ABDULMALIK A S, MANSOUR A, et al. Ultra wideband indoor positioning technologies: analysis and recent advances. Sensors, 2016, 16(5): 707.

[6] GU D, CHEN K S. Design and performance evaluation of wiimote-based two-dimensional indoor localization systems for indoor mobile robot control. Measurement, 2015, 66: 95–108.

[7] GARD V, JHAMB M. A review of wireless sensor network on localization techniques. International Journal of Engineering Trends and Technology, 2013, 4(4): 1049–1053.

[8] HUSSIEN H M, SHIFERAW Y N, TESHALE N B. Survey on indoor positioning techniques and systems. Proc. of the International Conference on Information and Communication Technology for Develoment for Africa, 2018: 46−55.

[9] HAN H, WANG J, LIU F, et al. An emergency seamless positioning technique based on ad hoc UWB networking using robust EKF. Sensors, 2019, 19(14): 3135.

[10] GHENDIR S, SBAA S, AL-SHERBAZ A, et al. Towards 5G wireless systems: a modified rake receiver for UWB indoor multipath channels. Physical Communication, 2019, 35(8): 100715.

[11] KIM Y H, CHOI M J, KIM E J, et al. Magnetic-map-matching-aided pedestrian navigation using outlier mitigation based on multiple sensors and roughness weighting. Sensors, 2019, 19(21): 4782.

[12] YU N, LI Y F, MA X F, et al. Comparison of pedestrian tracking methods based on foot-and waist-mounted inertial sensors and handheld smartphones. IEEE Sensors Journal, 2019, 19(18): 8160–8173.

[13] ELWELL J. Inertial navigation for the urban warrior. Proc. of the Digitization of the Battlesapce IV, 1999, 3709: 196–204.

[14] FOXLIN E. Pedestrian tracking with shoe-mounted inertial sensor. IEEE Computer Graphics and Applications, 2005, 25(6): 38–46.

[15] MENG X L, SUN S Y, JI L Y, et al. Estimation of center of mass displacement based on gait analysis. Proc. of the IEEE International Conference on Body Sensor Networks, 2011: 150−155.

[16] WANG Y S, SHKEL A M. Adaptive threshold for zero-velocity detector in ZUPT-aided pedestrian inertial navigation. IEEE Sensors Letters, 2019, 3(11): 1–4.

[17] HU G H, ZHANG W Z, WAN H, et al. Improving the heading accuracy in indoor pedestrian navigation based on a decision tree and Kalman filter. Sensors, 2020, 20(6): 1578.

[18] DENG Z H, WANG P Y, LIU T, et al. Foot-mounted pedestrian navigation algorithm based on BOR/MINS integrated framework. IEEE Trans. on Industrial Electronics, 2019, 67(5): 3980–3989.

[19] AHMAD I, HADRI A E, BENZIANE L, et al. Globally asymptotic attitude estimation for accelerated aerial vehicles. Aerospace Science and Technology, 2018, 84: 1175–1181.

[20] NARKHEDE P, JOSEPH R A N, KUMAR V, et al. Least square estimation-based adaptive complimentary filter for attitude estimation. Transactions of the Institute of Measurement and Control, 2019, 41(1): 235–245.

[21] LI Z, XU X B, JI M X, et al. Pedestrian positioning based on dual inertial sensors and foot geometric constraints. IEEE Trans. on Industrial Electronics, 2021, 69(6): 6401–6409.

[22] LAVERNE M, GEORGE M, LORD D, et al. Experimental validation of foot to foot range measurements in pedestrian tracking. Proc. of the 24th International Technical Meeting of the Satellite Division of the Institute of Navigation, 2011: 1386−1393.

[23] TJHAI C, O'KEEFE K. Comparing heading estimates from multiple wearable inertial and magnetic sensors mounted on lower limbs. Proc. of the IEEE International Conference on Indoor Positioning and Indoor Navigation, 2018: 206−212.

Biographies

CHENG Hao was born in 1998. He received his B.S. degree from Hefei University of Technology. He is pursuing his M.S. degree in Beihang University. His research interests are related to inertial navigation and indoor positioning.
E-mail: 13225517091@163.com

GAO Shuang was born in 1977. She received her Ph.D. degree from Beihang University. She is an associate professor in Beihang University. Her research interests are related to fiber optic gyroscope and navigation system.
E-mail: gaoshuang@buaa.edu.cn

CAI Xiaowen was born in 1981. She received her Ph.D. degree in optical engineering in Beihang University, China, in 2020. She is currently an associate professor with Xiangtan University. Her research interests are related to inertial navigation and integrated navigation.
E-mail: caixiaowen@xtu.edu.cn

WANG Yuxuan was born in 1992. He received his B.S. degree from Military Ecomomy Academy. He is pursuing his M.S. degree in Beihang University. His research interests are related to inertial navigation.
E-mail: sy2117129@buaa.edu.cn

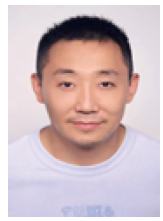

WANG Jie was born in 1990. He received his M.E. degree from Graduate School of the Second Institute of China Aerospace Science and Industry Corporation, Beijing, China. His research interests are related to inertial navigation and integrated navigation.
E-mail: wangquiler@163.com